Horizontal convection in shallow enclosures scales with height, not length, at low Rayleigh numbers

Sajjad Hossain*, Tony Vo, Gregory J. Sheard*

The Sheard Lab, Department of Mechanical and Aerospace Engineering, Monash University, VIC 3800, Australia

ABSTRACT

Horizontal convection is a distinct type of natural convection, where the flow is driven by non-uniform buoyancy supplied along a horizontal boundary. Horizontal convection has been studied in enclosures with aspect ratios (ratio of enclosure height H to length L) down to $O(10^{-1})$, though the flow dynamics and heat transfer in very shallow enclosures remain unexplored. This study employs a high-order spectral-element method and the Boussinesq buoyancy approximation to simulate horizontal convection in rectangular enclosures for aspect ratios $10^{-3} \le A = H/L \le 0.16$, over Rayleigh numbers $10 \le Ra \le 10^{16}$ and a fixed Prandtl number $Pr = 6.14$ representative of water. The flow is driven by imposing a linear temperature variation along the bottom boundary of the enclosure, and insulating temperature conditions on the remaining boundaries.

This work, for the first time, explores small aspect ratios towards the shallow-enclosure limit up to 100 times shallower than those studied previously to elucidate the effect of ocean-relevant confinement on horizontal convection. The Rayleigh number delineating the transition between the diffusion-dominated and convection-influenced regime is identified. The aspect ratio dependence of these Rayleigh numbers and their corresponding Nusselt numbers are found to follow power-law scalings $Nu \sim A$ and $Ra \sim A^{-4}$. These scalings illuminate a modified Nusselt number and Rayleigh number that govern horizontal convection at lower Rayleigh numbers, and reveal that height, rather than the horizontal length, governs the flow dynamics. Away from the side-walls the velocity and temperature profiles in these regimes exhibit self-similarity features and are well-described by the analytical solution for a one-dimensional horizontal channel flow driven by horizontal temperature gradient. A previously unseen behaviour is discovered whereby at aspect ratios $A \lesssim 0.1$, an increasingly broad horizontally uniform zone with no heat transfer into the base occupies the middle of the enclosure, thereby localising the heating and cooling to within a distance of approximately $4H$ of the sidewalls.

1. Introduction

Thermal convection includes heat and mass transfer by molecular diffusion and large-scale advection motion within a fluid. Research regarding thermally driven buoyancy flows is of great significance both in understanding geophysical flows and improvement of industrial process engineering applications [1]. The most extensively studied type of convection is the canonical Rayleigh–Bénard convection [2–6], where fluid flow is driven by destabilisation of the vertical thermal gradient owing to the forced differential heating of the horizontal layer of fluid with a cold upper layer. However, the present study investigates another distinctive mode of thermal convection where simultaneous heating and cooling along a horizontal boundary results in a horizontal thermal gradient that initiates a natural convection flow; this class of convection is known as horizontal convection [7].

Research interest in horizontal convection originated from geophysical and geological flows [8] as it can be regarded as a model providing insight into ocean overturning circulation [8–10]. It also informs industrial processes, for example, glass melting in furnaces [11,12]. A shallow enclosure with small aspect ratio is representative of a meridional segment of a typical ocean basin, whereas the imposed horizontal temperature gradient models the solar heating and ocean surface temperature. The oceanic circulation constitutes transportation of warm fluids from the tropical regions to high latitudes, where it cools and sinks, subsequently before an up-welling flow across the ocean basin completes the flow path [13]. Similarly, the fluid in horizontal convection undergoes advection while passing through a region of stable stratification towards an unstable region where vertical heat transport occurs away from the bottom boundary. One distinguishing feature of large-scale oceanic circulation is the formation of deep and

---

* Corresponding authors.
E-mail addresses: sajjad.hossain@monash.edu (S. Hossain), greg.sheard@monash.edu (G.J. Sheard).

Nomenclature

A	aspect ratio $A = H/L$
c_p	specific heat capacity of fluid
F_θ	heat flux
g	gravitational acceleration
$\hat{g}$	unit vector in direction of gravity
H	enclosure height
Nu	Nusselt number
Nu_{I-II}	threshold Nusselt number
Nu_H	horizontal Nusselt number
L	enclosure width; characteristic length of thermal forcing for horizontal convection
p	(pressure)
Pr	Prandtl number, $Pr = \nu/\kappa$
Ra	Rayleigh number based on imposed temperature difference across heated horizontal boundary
Ra_{I-II}	threshold Rayleigh number
Ra_H	horizontal Rayleigh number
t	(time)

$\boldsymbol{u}$	velocity vector
u	horizontal velocity component
x	Cartesian horizontal coordinate
y	Cartesian vertical coordinate

Greek symbols

α	volumetric thermal expansion coefficient
β	linear temperature gradient in (x) direction
$\delta\theta$	temperature difference imposed across horizontal boundary
$\delta\theta_H$	horizontal temperature difference imposed across horizontal boundary
κ_T	fluid thermal diffusivity
ν	fluid kinematic viscosity
θ	fluid temperature
ρ_0	reference density of fluid
θ_y	fluid temperature along (y) direction
θ_w	local bottom wall temperature

bottom water from relatively small regions of ocean surface [14]. This resembles the narrow vertical plume region in horizontal convection, whereas the simultaneous heating-cooling resembles the upwelling and downwelling features of the oceans.

While the manifestation of flow dynamics in horizontal convection under applied thermal forcing is increasingly well understood with a fixed enclosure aspect ratio, the characteristics of the key mechanisms under different aspect ratios, and particularly in shallow enclosures relevant to Earth's oceans, is less clear. Chiu-Webster et al. [12] investigated horizontal convection relevant to glass-melting processes and Earth's mantle. They considered the infinite-Prandtl number limit relevant to very viscous fluids at a range of aspect ratios $10^{-2} \le A \le 2$, with Ra up to 10^{10}. They reported a scaling of $Nu \sim Ra^{1/5}$ consistent with Rossby's [15] analysis, and provided evidence of an aspect ratio independence for $Ra > 10^7$. Sheard and King [16] used several aspect ratios, $0.16 \le A \le 2.0$ with an upper limit of $Ra = 10^{12}$ and $Pr = 6.14$ to study horizontal convection at high spatial resolution by using a spectral-element method. They reported aspect ratio dependence of Nu and boundary layer thickness at low Ra, whereas these became independent of aspect ratio for higher Ra once convective effects became dominant. For $A > 1$, the threshold Ra that separated the transition from diffusion-dominated to convection-influenced flow was found to be independent of aspect ratio. Besides, the development of unsteady flow resulted in an increase in the Nusselt number scaling exponent from 1/5 to approximately 1/4. It is evident that the confinement of small aspect ratios enclosures may influence the heat transport in horizontal convection flow.

The aim of this study is to investigate the effect of aspect ratio towards the shallow-enclosure limit. Consideration will be given to the dependence of Nu on aspect ratio and Rayleigh number, scaling of the flows towards the small aspect ratio limit, and the connection between these flows and one-dimensional channel flows.

This paper is structured as follows: § 2 describes the numerical approach and grid resolution study. The obtained heat transfer scalings in the context of small aspect ratio and proposed analytical solutions are described in § 3, and conclusions are drawn in § 4.

2. Numerical setup

The system under investigation is presented in Fig. 1, which consists of a rectangular enclosure of width L and height H filled with a fluid of density ρ_0, kinematic viscosity ν, thermal diffusivity κ, and volumetric expansion coefficient α. The flow is driven by imposition of a linear

temperature profile across the bottom boundary of the enclosure being $\delta\theta$ hotter at the right-hand end compared to the left-hand end, while insulating temperature conditions are imposed on the remaining boundaries (a zero temperature gradient normal to the walls). A no-slip condition (zero velocity) is imposed on all boundaries. The buoyancy is modelled with the Boussinesq approximation, which implies that the density differences in the fluid are disregarded except through the contribution of buoyancy in the momentum equation. Hence, the energy equation simplifies to a scalar advection-diffusion equation for temperature which is evolved in accordance with the velocity field. The fluid temperature is related linearly to the density via thermal expansion coefficient α. The governing equations are therefore written as

$$\frac{\partial \boldsymbol{u}}{\partial t} = -(\boldsymbol{u} \cdot \nabla)\boldsymbol{u} - \nabla p + Pr\,\nabla^2 \boldsymbol{u} + Pr\,Ra\,\hat{\boldsymbol{g}}\,\theta, \tag{1}$$

$$\nabla \cdot \boldsymbol{u} = 0, \tag{2}$$

$$\frac{\partial \theta}{\partial t} = -(\boldsymbol{u} \cdot \nabla)\theta + \nabla^2 \theta, \tag{3}$$

where t is time, θ is temperature, p is pressure, $\boldsymbol{u}$ is the velocity vector and $\hat{\boldsymbol{g}}$ is a unit vector in the direction of the gravity. In Eqs (1)–(3), lengths, time, velocity, pressure and temperature are respectively scaled by L, L^2/κ, κ/L, $\rho_0\kappa^2/L^2$ and $\delta\theta$.

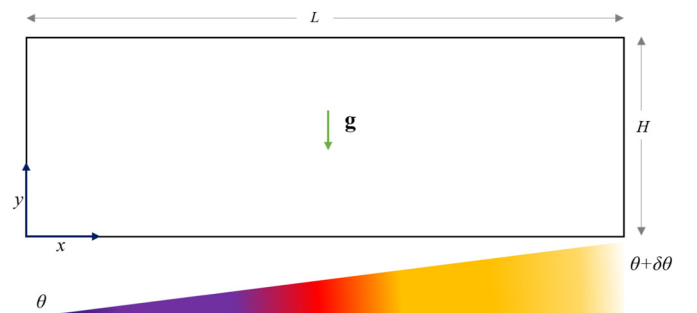The Rayleigh number characterizing the ratio of buoyancy to thermal and molecular dissipation is

Fig. 1. A schematic representation of the computational domain under investigation with the prescribed boundary conditions along each of the boundary. The range of aspect ratios used throughout this study is $0.001 \le H/L \le 0.16$.

$$Ra = \frac{g\alpha\delta\theta L^3}{\nu\kappa}, \tag{4}$$

where g is the gravitational acceleration. The ratio between fluid viscosity ν and thermal diffusivity is parameterized by Prandtl number

$$Pr = \nu/\kappa, \tag{5}$$

and throughout this study $Pr = 6.14$ is used, representing water at laboratory conditions (25°C). The Nusselt number denotes the ratio of convective to conductive heat transfer, and is defined as

$$Nu = \frac{F_\theta L}{\rho_0 c_p \kappa \delta\theta}, \tag{6}$$

with heat flux

$$F_\theta = \kappa\rho_0 c_p \overline{\frac{\partial\theta}{\partial y}}, \tag{7}$$

where c_p is the specific heat capacity of the fluid, and $\overline{\partial\theta/\partial y}$ is the averaged absolute vertical temperature gradient along the forcing boundary.

2.1. Mesh dependence

The governing Eqs. (1)–(3) were solved on a two-dimensional domain using a high-order solver based on a nodal spectral element method for spatial discretisation and a third-order time integration scheme based on backward-differencing [17]. This solver has been employed and validated in previous studies featuring different aspects of horizontal convection flows [16,18–20]. Meshes were constructed for aspect ratios over $0.001 \le A \le 0.16$. The number of quadrilateral spectral elements in the meshes varied between 296 and 4128. The elements were compressed towards the side walls; specifically adjacent to the hot bottom end boundary to ensure that the flows were resolved. The highest aspect ratio considered in this study was $A = 0.16$, which matches the most widely used shallow enclosure and overlapping the shallowest enclosure, $A = 0.1$ (used in [21]), mentioned in previous horizontal convection experiments.

A thorough grid resolution study was conducted for all the meshes to determine the optimal polynomial order to be employed within each spectral element. The error (relative to the highest polynomial order) percentage in the $\mathscr{L}^2$ norm, average temperature of the enclosure and Nusselt number are used to measure the convergence of the solutions. The error of each parameter is shown in Fig. 2. Considering the $\mathscr{L}^2$ norm, the error dropped below 10^{-5}% for polynomial orders $N \ge 5$. The errors reduced to approximately 10^{-7}% with a polynomial degree of 9. The errors for average enclosure temperature and Nusselt number were also less than 0.1% for polynomial orders $N \ge 5$. Balancing the trade-off between computational cost and accuracy, a polynomial order of 5 was selected for the remainder of the study.

3. Result and discussion

3.1. Heat transfer regimes of horizontal convection

The Nusselt number was calculated from the vertical thermal flux distribution along the bottom horizontal boundary of the enclosure for each aspect ratio, and these were plotted against the Rayleigh number. Fig. 3 presents the change of Nusselt numbers with increasing Rayleigh numbers computed throughout the range of aspect ratios. Based on the characteristics of Nusselt number with the increase of Rayleigh number, the data can be divided into three zones. At low Rayleigh numbers, Nusselt numbers at each aspect ratio are independent of the Rayleigh number. In this regime, Nusselt numbers are only dependent on aspect ratio, and this range of Rayleigh numbers is referred to as the diffusion-dominated or conduction regime. At each aspect ratio, there is a Rayleigh number beyond which the Nusselt number displays a rapid

increase. This regime will be referred to as the transition regime. Beyond this regime, the Nu data collapse onto a single curve at higher Rayleigh numbers where convection-dominated flows are observed. The convective regime is seen to set in at relatively low Ra for $A = 0.16$, with dividing Rayleigh number increasing with decreasing A. This is consistent with the behavior reported at larger aspect ratios in [16], and supports the view that increasing the degree of enclosure confinement, (i.e. decreasing A) delays the onset of the regimes is to higher Rayleigh numbers. Beyond these qualitative behaviours that are consistent with aspect-ratio dependence reported in the literature [16], the present penetration to much lower aspect ratios permits, for the first time, scalings towards the limit of vanishing aspect ratio to be revealed.

Scalings between Rayleigh number, Nusselt number and aspect ratio have been determined to elucidate the behavior of horizontal convection in shallow enclosures. In the diffusion-dominated regime, Nusselt number scales with aspect ratio as $Nu \propto A^1$. The onset of the transition regime is demarked by a threshold Rayleigh number, Ra_{I-II}, which has a corresponding Nusselt number Nu_{I-II}. To identify the threshold between the diffusion-dominated and transitional regimes, Ra_{I-II} is defined when Nusselt number has deviated by 5% from its Ra-independent value. The threshold Rayleigh number was then found to scale as $Ra_{I-II} \sim A^{(-3.9481 \pm 0.000673)}$. Combining this with $Nu \sim A^1$ reveals the threshold scaling, $Nu \sim Ra_{I-II}^{-1/4}$. In the convection dominated regime beyond the transition regime, the obtained scaling between Rayleigh and Nusselt numbers becomes $Nu \sim Ra^{1/4}$. Considering the mean and SEM value this scaling can be written as $Nu \sim Ra^{(0.2461 \pm 0.0039)}$.

The velocity and temperature fields corresponding to these three regimes illustrate the flow dynamics inside the range of shallow enclosures. The linear temperature gradient imposed on the horizontal base of the shallow enclosure provides the heat-transfer from the boundary to the adjacent fluid through molecular conduction. Eventually, a horizontal thermal boundary layer develops and carries the heat along the bottom boundary. The progression towards unsteady conditions is most prominent in the hot end of the enclosure.

Figs. 4 and 5 respectively show the horizontal velocity and temperature fields in the vicinity of the hot right-hand end of the closure for $A = 0.08$ at different Rayleigh numbers chosen to visualize each of the three regimes. Figs. 4(a) and 5(a) show the diffusion-dominant regime, where the flow features a symmetric pattern throughout the
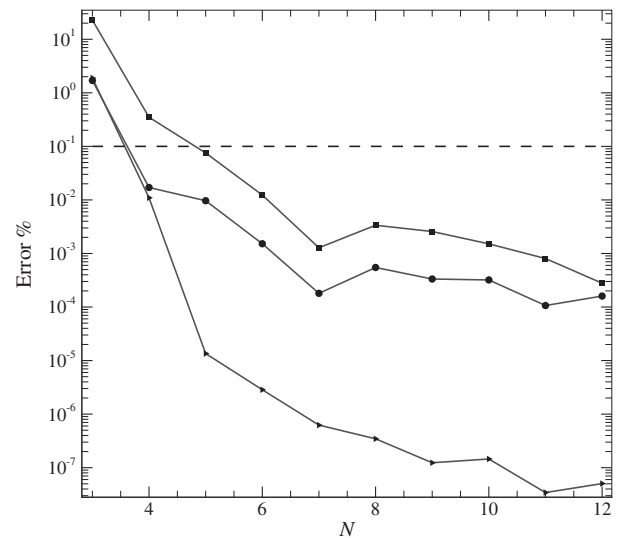

Fig. 2. Errors of the $\mathscr{L}^2$ norm (triangles), average enclosure temperature (circle) and Nusselt number (square) plotted against the degree of polynomial order (N) imposed on the spectral elements. The flow conditions for this study were $Ra = 10^{10}$ and $Pr = 6.14$.
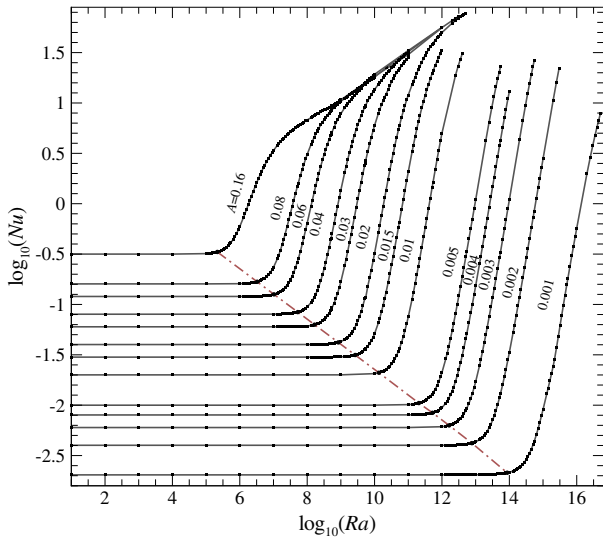
Fig. 3. A comparison of the $\log_{10}(Nu)$ for $0.001 \leq A \leq 0.16$ range while varying the $\log_{10}(Ra)$. The dashed line refers to the onset of transition regimes for every aspect ratio.
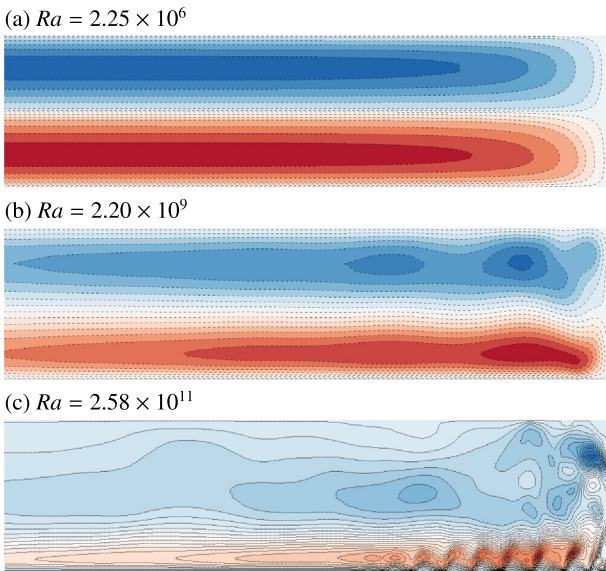
(a) $Ra = 2.25 \times 10^6$

(b) $Ra = 2.20 \times 10^9$

(c) $Ra = 2.58 \times 10^{11}$

Fig. 4. Horizontal velocity contour plots for $A = 0.08$ representing (a) diffusion-dominated regime, (b) transition regime and (c) convection-influenced regime while focused to the hot-end of the horizontal bottom boundary. Dark to light shaded contours show respective maximum and minimum values of U for (a), (b) and (c) ranging over ± 8, ± 1600 and ± 4600 with 13, 15 and 22 contour levels plotted, respectively.

whole enclosure and remains time independent. Figs. 4(b) and 5(b) show that in the transitional regime the flow dynamics change as this symmetry is lost: the formation of a thermal boundary layer is evident, transporting colder fluid towards the hotter end. The loss of the symmetry is seen via the shift of the fastest fluid closer to the bottom boundary and the hot end, which gives rise to the vertical jet transporting heat and fluid away from the bottom boundary. While transporting heat upwards and horizontally alongside the enclosure top boundary, the fluid gradually cools, descending diffusively and stably towards the cold end of the bottom-boundary. In this regime, the flow pattern is mostly symmetric about the horizontal mid-plane but skewed adjacent to the vertical hot-end wall as shown in Fig. 4(c). With an increase in Rayleigh number, the thermal boundary layer becomes
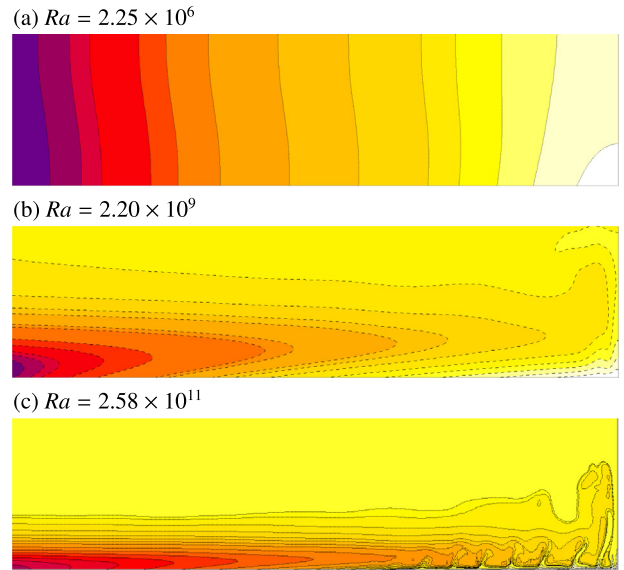
(a) $Ra = 2.25 \times 10^6$

(b) $Ra = 2.20 \times 10^9$

(c) $Ra = 2.58 \times 10^{11}$

Fig. 5. Temperature contour plots for $A = 0.08$ representing (a) diffusion-dominated regime, (b) transition regime and (c) convection-influenced regime while focused to the hot-end of the horizontal bottom boundary. Dark to light shaded contours show values between $-0.45 \leq \theta \leq 0.45$. In (a), (b) and (c), 21, 25 and 21 contour levels are plotted, respectively.

thinner (in this regime the boundary layer is sufficiently thin that the top boundary no longer modifies the convective heat transport) and eruption of the plumes are evident at the hot end of the enclosure, which can be observed from Fig. 5(c).

Within the convection-influenced regime, fully developed plumes are visible and the returning flow commences after this regime to complete the circulation inside the shallow enclosure. Owing to the linear temperature forcing, the multiple thin plumes that originate from the fragmentation of the single plume do not possess sufficient energy to reach the top boundary. As a result, fractions of the plume undergo convection processes along the middle of the shallow enclosures and the entraining cold fluid leads towards a localized circulation entrapped within the rightmost side of the enclosure. The convection-dominated regime exhibits flows that can be either steady-state, time-periodic or chaotic. Fig. 6 presents a regime map of the Rayleigh number-aspect ratio parameter space identifying these states. This map marks the diffusion-dominated regime (I) and convective regime (III) as shaded zones. The region between the shaded zones represents the transition regime (II), which follows the scaling of $Ra \sim A^{-4}$. This regime map reveals the steady to unsteady features of the flow for the three different regimes. As can be seen from Fig. 6, the flow remains steady in the diffusion-dominated regime, whereas it becomes unsteady in the convection-influenced regime. Initially, the flow remains steady in the transition regime, but as it approaches the convection-influenced regime (III) it becomes unsteady (periodic flow).

3.2. Self-similarity in horizontal convection

The variation of the Nusselt numbers for all A-values throughout the range of Rayleigh numbers emphasizes self-similar features at lower-Ra values. Based on the low-Ra/low-A scalings of $Nu \sim A$ and $Ra \sim A^{-4}$, the data from Fig. 3 can be rescaled and plotted as Nu/A against RaA^4, the outcome of which is shown in Fig. 7. For lower values of RaA^4, the corresponding values of Nu/A can be seen to have collapsed onto a universal curve for all aspect ratios. This collapse demonstrates that the flow in this regime is governed by the modified Rayleigh number RaA^4. Considering the scaled Nusselt and Rayleigh numbers, defined here as Nu_H and Ra_H, respectively, Eq (8) and (9)
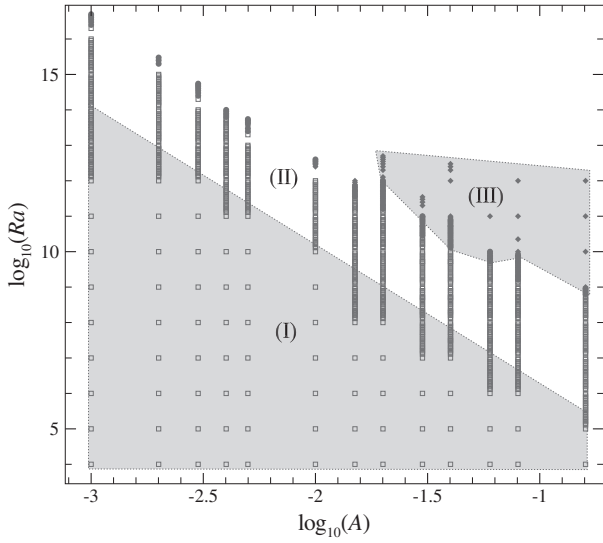
Fig. 6. A regime map of Ra–A parameter space computed considering the log values. Symbols denote points at which data was acquired, with open symbols showing steady solution and filled symbols (circles for periodic flow, and diamonds for aperiodic flow) unsteady solutions, respectively. The marked regions (I), (II) and (III) represent the diffusion-dominated, transition and convection-influenced regimes, respectively.
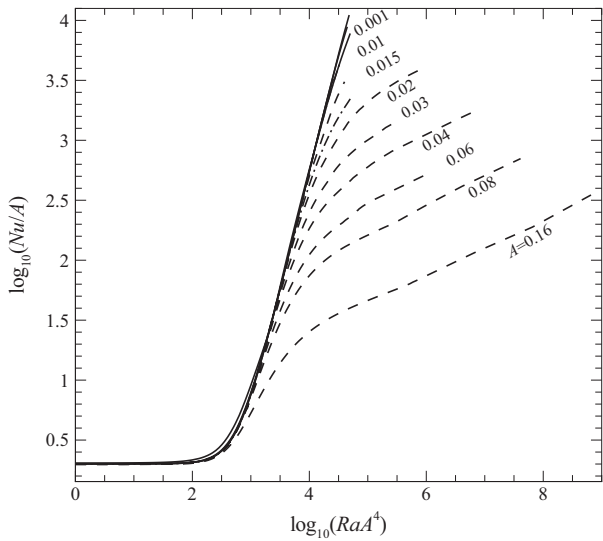

Fig. 7. The Nu–Ra plot has been rescaled to show $\log_{10}(Nu/A)$ against $\log_{10}(RaA^4)$ to investigate the self similarity features in the low-Ra number region.

$$Nu_H = \frac{Nu}{A} = \frac{F_\theta L}{\rho_0 c_p \kappa (\delta\theta A)} = \frac{F_\theta L}{\rho_0 c_p \kappa \delta\theta_H} \tag{8}$$

$$Ra_H = RaA^4 = \frac{\alpha g \,\delta\theta L^3}{\nu\kappa}\frac{H^4}{L^4} = \frac{g\alpha(\delta\theta A)}{\nu\kappa}H^3 = \frac{g\alpha\delta\theta_H}{\nu\kappa}H^3, \tag{9}$$

it is revealed that low-aspect ratio horizontal convection is govenered by the enclosure height rather than its horizontal length. Here, $\delta\theta_H$ refers to the temperature difference along a portion of the bottom boundary of length H. Notice that the characteristic length quantity L appearing in the horizontal Rayleigh number definition has been replaced by H through this analysis. The corollary to this is that in very shallow enclosures, horizontal convection will be insensitive to the overall length of the enclosure, rather its behaviour will be controlled by the enclosure height and the horizontal temperature gradient acting
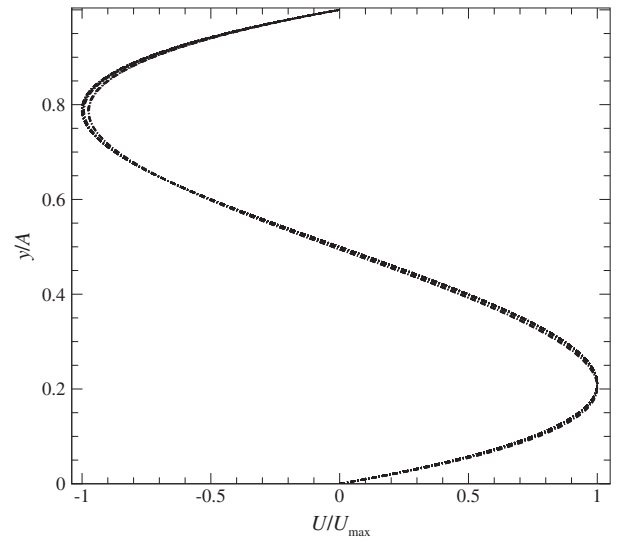

Fig. 8. The horizontal velocity profiles generated from different locations throughout the horizontal bottom boundary are plotted for modified Rayleigh number, $\log_{10}(Ra_H) = 1.75$ and $10^{-3} \le A \le 0.16$.

over that same scale. As can be seen from Fig. 7, after $\log_{10}(RaA^4) = \log_{10}(Ra_H) \approx 1.75$ the Nu/A values for all aspect ratios start branching off for $\log_{10}(Ra_H) \gtrsim 1.75$, starting with the highest $A = 0.16$ and then in descending order to the lowest $A = 0.001$ with increasing Rayleigh number. This resembles the opposite of the collapse within the convection dominated regime seen in Fig. 3.

Attention is now turned to profiles of the horizontal velocity component and temperature extracted at various horizontal locations within the enclosures. The locations are selected at different distances from the hot end, and are plotted against the height from the base. The extracted velocities were normalized by the maximum velocity value from each profile U/U_{max}, while the vertical coordinate was normalized by enclosure height (y/A), based on the dimensionless y coordinate. Results are shown in Fig. 8, which presents the combined velocity profiles for all aspect ratios at a single value of RaA^4 within the collapsed regime. The normalized profiles exhibit a strong collapse to a universal profile, implying a self-similarity in the velocity fields in this regime. By observing the extracted velocity data for all aspect ratios throughout different locations (which are expressed in terms of the distance x' from the hot end-wall) along the horizontal boundary, it is evident from Fig. 9 that beyond a distance of approximately $4H$, all trends collapse to a single curve. This demonstrates that the effects of the sidewalls in conduction-dominated horizontal convection are confined to within $4H$ from the wall, and this distance scales with height, rather than the horizontal enclosure length. This previously unreported behavior emerges in enclosures having $L \gtrsim 8H$, or $A = H/L \lesssim 1/8$, i.e. $A \lesssim 0.125$, which is shallower than the most widely studied enclosure ($A = 0.16$) investigated previously.

Similarly, temperature profiles relative to the local bottom wall temperature (θ_w), were extracted and normalized by the vertical temperature difference ($\theta_y - \theta_w$) of each profile. The results are shown in Fig. 10. In contrast to the velocity contour scaling, the temperature contours for all aspect ratios are not well-collapsed as the obtained values in the vicinity of the hot-end wall seems to deviate from the rest of the data sets. However, similar to the velocity contours, the temperature contours also demonstrate the self-similarity feature beyond the $4H$ distance from the end wall for all aspect ratios.

The observation of a horizontally independent central region of the flow and temperature fields raises the question as to whether that region can be described analytically. To address this question, the analytical solution to the related problem of natural convection within an
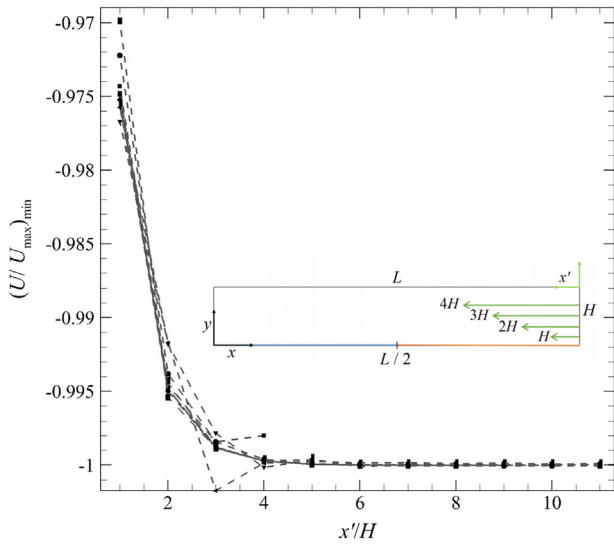
Fig. 9. Minimum values of the scaled velocity plotted with the distance form hot-end wall. The distance is expressed in terms of the height of the enclosure. The inset figure demonstrates how the distance from the hot-end is defined as a function of enclosure height.

infinite horizontal channel under a uniform horizontal thermal gradient and zero net horizontal flow is sought. The analytical solutions are derived from the momentum and energy equations as stated in Eqs (10), (11) and (12)

$$\frac{\partial u}{\partial t} + u\frac{\partial u}{\partial x} + v\frac{\partial u}{\partial y} = -\frac{1}{\rho}\frac{\partial p}{\partial x} + \nu\left(\frac{\partial^2 u}{\partial x^2} + \frac{\partial^2 u}{\partial y^2}\right),$$

(10)

$$\frac{\partial v}{\partial t} + u\frac{\partial v}{\partial x} + v\frac{\partial v}{\partial y} = -\frac{1}{\rho}\frac{\partial p}{\partial y} + \alpha(-g)\theta + \nu\left(\frac{\partial^2 v}{\partial x^2} + \frac{\partial^2 v}{\partial y^2}\right)$$

(11)

$$\frac{\partial \theta}{\partial t} + u\frac{\partial \theta}{\partial x} + v\frac{\partial \theta}{\partial y} = \kappa\left(\frac{\partial^2 \theta}{\partial x^2} + \frac{\partial^2 \theta}{\partial y^2}\right).$$

(12)

Normalising length, velocity and temperature respectively by H/A, $\kappa A/H$ and $\delta\theta$, the analytical solution representing the horizontal velocity and temperature fluctuation can be expressed in Eqs (13) and (14), respectively, where y is set according to the coordinate system introduced in Fig. 1.

$$U = \frac{Ra\,A^3}{12}(2y^3 - 3y^2 + y)$$

(13)

and

$$\theta' = \frac{Ra\,A^5}{24}\left(\frac{y^5}{5} - \frac{y^4}{2} + \frac{y^3}{3}\right).$$

(14)

This solution was verified against the simulation results for all aspect ratios. Fig. 11 presents error propagation plots of horizontal velocity and temperature fluctuation values calculated from the differences between the analytical solution and the simulation results for $\log_{10}(Ra_H) = 1.75$. The maximum difference between the analytical and simulation results of $A = 0.08, 0.015$ and 0.001 for the horizontal velocity are approximately 2.95%, 2.16% and 0.01%, and the temperature fluctuation difference are approximately 1.24%, 2.36% and 1.40%, respectively. The analytical solution is valid beyond the $4H$ distance from the end walls found below $H/L \approx 1/8$ within the diffusion-dominated flow regime with a Ra-limit of $\log_{10}(Ra_H) = \log_{10}(Ra(H/L)^4) = 1.75$.
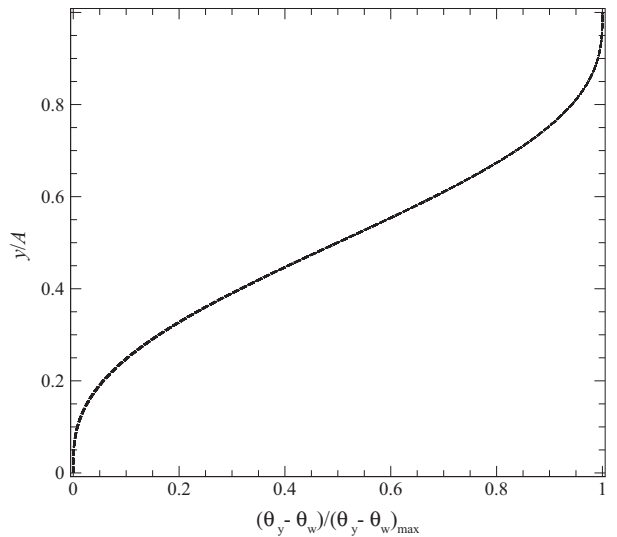
3.3. Confined heating and cooling regions

The horizontal length independence and self similarity of shallow

(a) Within $4H$ of side walls
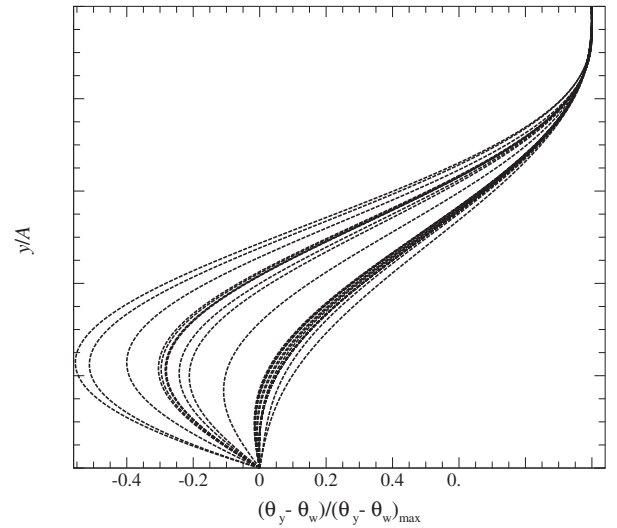
(b) Beyond $4H$ of each side wall

Fig. 10. The temperature profiles generated from different locations throughout the horizontal bottom boundary are plotted (a) for locations within the $4H$ distance from hot-side end wall, and (b) for locations beyond the $4H$ at a modified Rayleigh number, $\log_{10}(Ra_H) = 1.75$ and $10^{-3} \le A = H/L \le 0.16$.

enclosure horizontal convection towards the one-dimensional channel flow discussed in § 3.2 invites more exploration. This section investigates the fluctuating part of the temperature throughout the aspect ratio range $10^{-3} \le A \le 0.16$, motivated by the observation that Eq. (14) describes a zero vertical derivative of temperature at the bottom wall ($y = 0$), that predicts no heat transfer through the base. Fig. 12 presents the obtained temperature fields for three representative aspect ratios from the range $10^{-3} \le A = H/L \le 0.16$. As aspect ratio decreases, a region of horizontally independent temperature contours develops in the interior of the enclosure. This region becomes more prominent as the aspect ratio gets smaller: notice the horizontal isotherms along the majority of the domain, with changes confined to the near-wall regions. This supports the earlier finding that the temperature fluctuation is indeed horizontally independent away from the endwalls. This horizontally independent region corresponds to the portion of the shallow enclosure that agrees with the analytical channel flow solution presented in Eq. (14), which has zero heat flux at the bottom boundary. Hence heating and cooling are confined to the end-wall regions where the temperature fluctuation contours are not horizontally
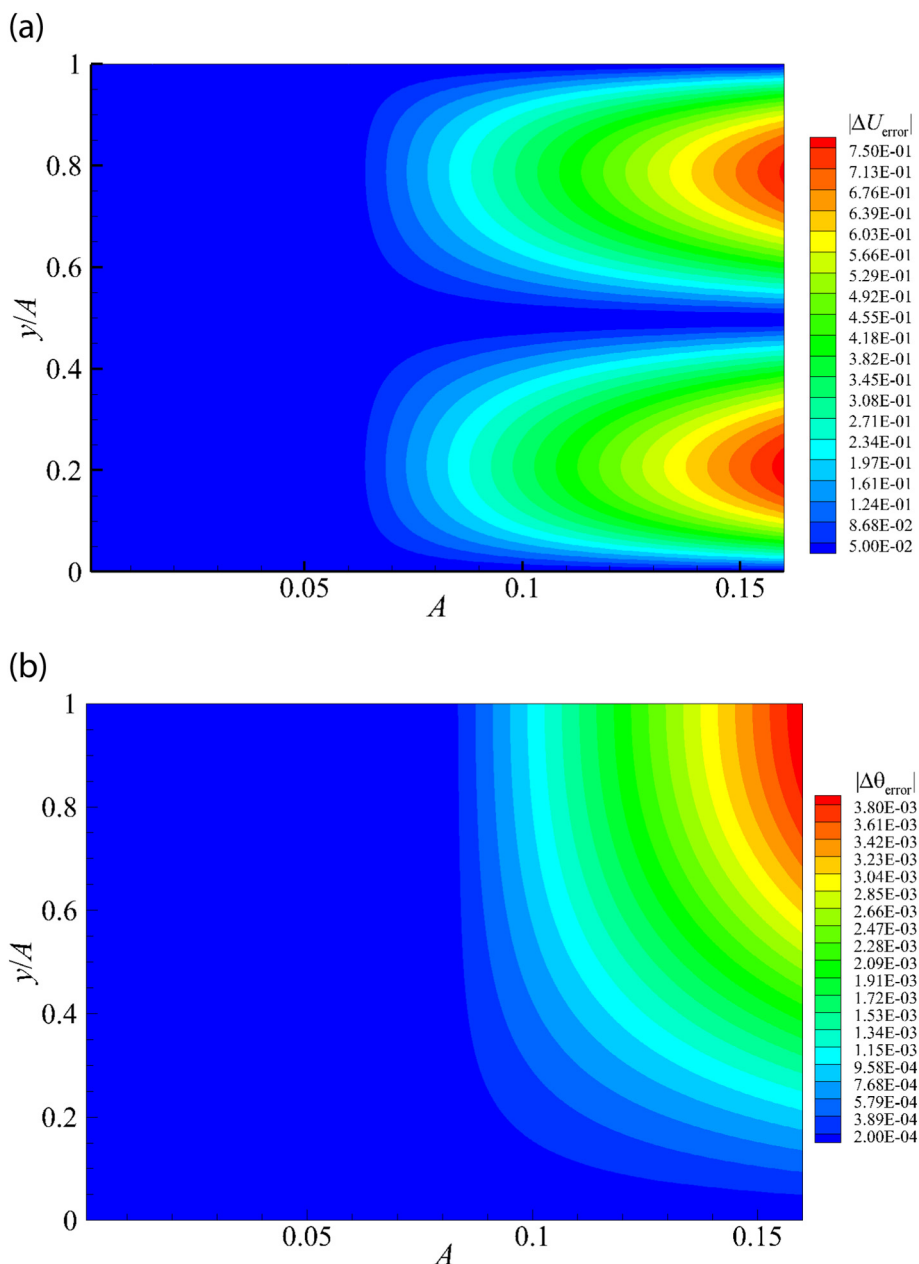
(a)

(b)

Fig. 11. Propagation of the absolute error between the dataset obtained from simulation and analytical solution is plotted through 2D-triangulation. The error propagation of (a) horizontal velocity and (b) temperature fluctuation are plotted with scaled vertical coordinates and the aspect ratios.

independent. It has been found that the turnover of the flow at each end of the enclosure is confined to within 4H of each end wall. As can be seen from Fig. 12, the previous horizontal convection studies had enclosure aspect ratios too large ($A \geq 0.16$) to detect this significant behaviour. This is reinforced in Fig. 12 by the inclusion of vertical dashed lines highlighting the positions 4H in from each side wall in each of the three frames (noting that the vertical scale is stretched differently in each frame for visualization purposes). In Fig. 12(a), $A = H/L = 0.16$; in other words, a distance 4H from one end-wall is less than 4H from the other end wall - there is no room for this horizontally independent zone at this aspect ratio, or any aspect ratio $A \gtrsim 0.125$, which explains why this feature has not been observed in previously reported horizontal convection experiments.

4. Conclusions

Horizontal convection at ocean-relevant shallow enclosure aspect ratios have been investigated for a wide range of Rayleigh numbers with $Pr = 6.14$ by employing high-resolution spectral element simulations with a linear temperature profile applied along the horizontal boundary. Different regimes and the respective heat transfer scalings between Nu, Ra and A are revealed to understand the effect on enclosure confinement. A threshold Ra identified the transition from the diffusion-dominated regime to convection-dominated regime and was found to scale with A^{-4}, whereas the corresponding Nusselt number at the threshold was proportional to A. These scalings led to modified parameters, Nu_H and Ra_H, which govern the low-Ra conduction-dominated regime. These modified parameters revealed that low-Ra shallow-enclosure horizontal convection is insensitive to the enclosure width, and is only controlled by its height.

The velocity and temperature contours demonstrate self-similar behaviour in velocity and temperature profiles beyond a distance of 4H from each enclosure end-wall for all aspect ratios. In this interior region, normalized velocity and temperature profiles are found to follow
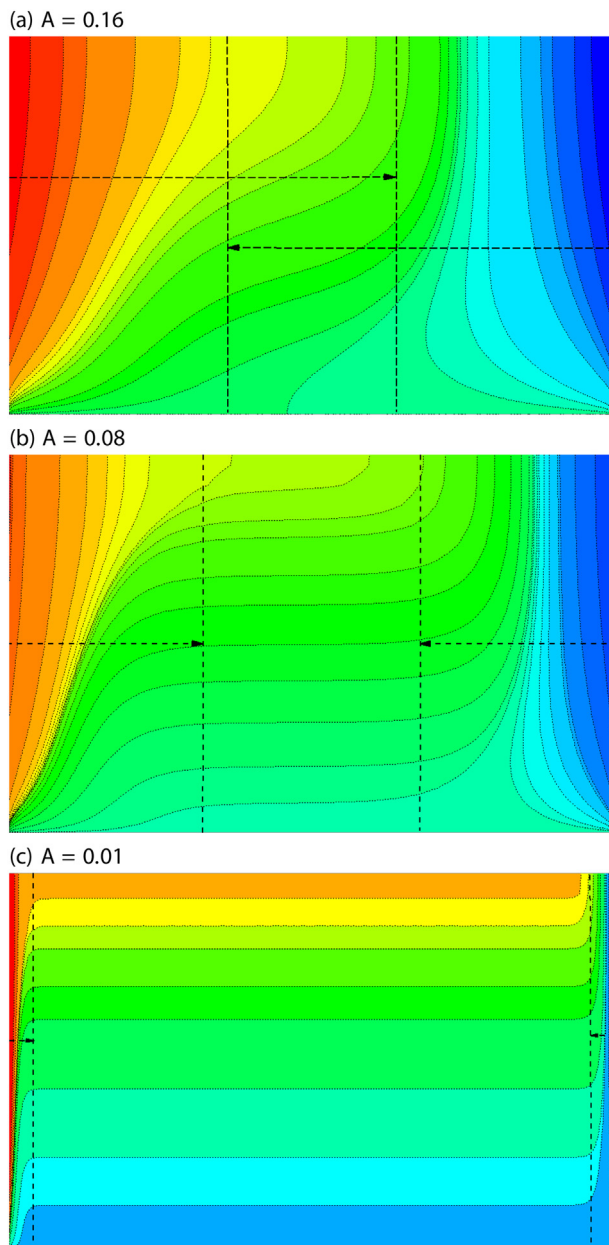
(a) A = 0.16

(b) A = 0.08

(c) A = 0.01

Fig. 12. Temperature fluctuation contours of (a) $A = 0.16$, (b) $A = 0.08$ and (c) $A = 0.01$ for a modified Rayleigh number of $\log_{10}(Ra_H) = 1.75$. Red to blue shaded contours show respective maximum-minimum values of temperature fluctuation for (a), (b) and (c) are $\pm 3 \times 10^{-3}$, $\pm 6 \times 10^{-2}$ and $\pm 8 \times 10^{-2}$ with contour levels of 12, 30 and 22. The vertical height of the contour plots has been increased to aid visualization. The dashed lines and arrows represent the $4H$ regions from left and right walls of the enclosure. (For interpretation of the references to colour in this figure legend, the reader is referred to the web version of this article.)

the analytical solution of a one-dimensional horizontal channel with zero net flow driven by a uniform horizontal thermal gradient.

Furthermore, a previously unseen behaviour is discovered, whereby the turning of the flow at the enclosure sidewalls is confined to a small region near the walls, while away from the walls the flow is horizontally independent. The sidewall effects are confined to within a distance of approximately four times the enclosure height. This reveals that the most widely used and the shallowest enclosure previously investigated in the literature is not sufficiently shallow to capture this phenomenon.

Acknowledgements

References

[1] F. Pigeonneau, J.-M. Flesselles, Practical laws for natural convection of viscous fluids heated from above in a shallow cavity, Int. J. Heat Mass Transf. 55 (2012) 436–442.
[2] G. Ahlers, S. Grossmann, D. Lohse, Heat transfer and large scale dynamics in turbulent Rayleigh-Bénard convection, Rev. Mod. Phys. 81 (2009) 503.
[3] L.P. Kadanoff, Turbulent heat flow: structures and scaling, Phys. Today 54 (2001) 34–39.
[4] F. Chillò, J. Schumacher, New perspectives in turbulent Rayleigh-Bénard convection, Eur. Phys. J. E Soft Matter 35 (2012) 1–25.
[5] H. Bénard, Les tourbillons cellulaires dans une nappe liquide propageant de la chaleur par convection: en régime permanent, Gauthier-Villars, 1901.
[6] L. Rayleigh, Lix. on convection currents in a horizontal layer of fluid, when the higher temperature is on the under side, Lond. Edinb. Dublin Philos. Mag. J. Sci. 32 (1916) 529–546.
[7] S. Grossmann, D. Lohse, Scaling in thermal convection: a unifying theory, J. Fluid Mech. 407 (2000) 27–56.
[8] G.O. Hughes, R.W. Griffiths, Horizontal convection, Annu. Rev. Fluid Mech. 40 (2008) 185–208.
[9] M.E. Stern, Ocean Circulation Physics, 246 Academic Press New York, 1975.
[10] J.C. Mullarney, R.W. Griffiths, G.O. Hughes, Convection driven by differential heating at a horizontal boundary, J. Fluid Mech. 516 (2004) 181–209.
[11] G. HJJ, H. PD, O. JR, Convection by a horizontal thermal gradient, J. Fluid Mech. 586 (2007) 41–57.
[12] S. Chiu-Webster, E.J. Hinch, J.R. Lister, Very viscous horizontal convection, J. Fluid Mech. 611 (2008) 395–426.
[13] F. Paparella, Turbulence, horizontal convection, and the Ocean's meridional overturning circulation, in: F. Ancona, P. Cannarsa, C. Jones, A. Portaluri (Eds.), Mathematical Paradigms of Climate Science, 15 Springer, 2016.
[14] H. Stommel, On the smallness of sinking regions in the ocean, Proc. Natl. Acad. Sci. U. S. A. 48 (1962) 766.
[15] H.T. Rossby, On thermal convection driven by non-uniform heating from below: an experimental study, Deep-Sea Res. Oceanogr. Abstr. 12 (1965) 9–16.
[16] G.J. Sheard, M.P. King, Horizontal convection: effect of aspect ratio on Rayleigh number scaling and stability, Appl. Math. Model. 35 (2011) 1647–1655.
[17] L.P. Kadanoff, High-order splitting methods for the incompressible navier-stokes equations, J. Comput. Phys. 97 (1991) 414–443.
[18] T. Tsai, W.K. Hussam, A. Fouras, G.J. Sheard, The origin of instability in enclosed horizontally driven convection, Int. J. Heat Mass Transf. 94 (2016) 509–515.
[19] G.J. Sheard, W.K. Hussam, T. Tsai, Linear stability and energetics of rotating radial horizontal convection, J. Fluid Mech. 795 (2016) 1–35.
[20] Z.Y. Ng, T. Vo, G.J. Sheard, Stability of the wakes of cylinders with triangular cross-sections, J. Fluid Mech. 844 (2018) 721–745.
[21] O. Shishkina, Mean flow structure in horizontal convection, J. Fluid Mech. 812 (2017) 525–540.